Charge distributions of fission fragments of low- and high-energy fission of Fm, No, and Rf isotopes

H. Pașca,[1,2] A. V. Andreev,[1] G. G. Adamian,[1] and N. V. Antonenko[1,3]
[1]*Joint Institute for Nuclear Research, 141980 Dubna, Russia*
[2]*"Babeș-Bolyai" University, Faculty of Physics, 400084 Cluj-Napoca, Romania*
[3]*Mathematical Physics Department Tomsk Polytechnic University, 634050 Tomsk, Russia*

(Received 12 February 2018; published 26 March 2018)

The charge (mass) distributions of fission fragments resulting from low- and high-energy fission of the even-even nuclei $^{254-260,264}$Fm, $^{258-264}$No, and $^{262-266}$Rf are studied with the statistical scission-point model. The calculated results are compared with the available experimental data. In contrast to the experimental data, the calculated mass distribution for ^{258}Fm(s.f.) is strikingly similar to the experimental one for ^{257}Fm(s.f.). The transformation of the shape of charge distribution with increasing isospin and excitation energy occurs gradually and in a similar fashion like that of the mass distribution, but slower. For ^{254}Fm(i.f.), ^{257}Fm(n_{th},f), and ^{260}Fm(s.f.), the unexpected difference (symmetric or asymmetric) between the shapes of charge and mass distributions is predicted for the first time. At some critical excitation energy, the saturation of the symmetric component of charge (mass) yields is demonstrated.

DOI: 10.1103/PhysRevC.97.034621

I. INTRODUCTION

The mass distributions in low-energy fission of nuclei U–Cf are known to be mostly asymmetric [1]. The first observation of the onset of symmetric distribution was made in the spontaneous fission of ^{257}Fm [1,2]. For ^{258}Fm, the spontaneous fission results in the unexpected narrow symmetric mass distribution [3]. The symmetric distributions have been also observed in the spontaneous fission of ^{259}Fm, ^{259,260}Md, ^{258,262}No, and ^{259}Lr [1]. The thermal-neutron-induced fission of ^{256,257}Fm [1] leads to the symmetric mass distribution, but with larger width than that in spontaneous fission of ^{258}Fm. For spontaneous fissioning Fm isotopes, an evolution of mass-yield shape with increasing isospin occurs suddenly as demonstrated in Ref. [3]. However, a survey of literature reveals a lack of data on the charge distributions of fission products in the spontaneous and induced fission of Fm, No, and Rf, particularly as a function of isospin and excitation energy. It is interesting to answer the question if there is the difference between the shapes (symmetric or asymmetric) of charge and mass distributions in fission of nuclei in this transeinsteinium region. Thus, one can focus the studies on the isospin and excitation energy dependencies of the charge yields.

In this paper, we employ the improved version of the statistical scission-point model [4–6], to study the evolution of the charge (mass) distribution of fission fragments with increasing mass number and excitation energy of even-even isotopes of $^{254-260,264}$Fm, $^{258-264}$No, and $^{262-266}$Rf. Our aim is to predict the transformation of the shape of charge distribution with increasing neutron number and excitation energy.

II. MODEL

The statistical scission-point model [4–6] relies on the assumption that the statistical equilibrium is established at scission of fissioning nucleus where the observable characteristics of fission are formed. The reliability of this conclusion is supported by a good description of various experimental data (mass, charge, kinetic energy distributions, and neutron multiplicity) with the scission-point models [4–16]. The dinuclear system (DNS) [13,17–28] is shown to be well suited for describing the scission configuration. So, the fissioning nucleus at scission-point is modeled by two nearly touching coaxial ellipsoids—fragments of the DNS with mass (charge) numbers A_L (Z_L) and A_H (Z_H) for the light (L) and heavy (H) fragments, respectively. Here, $A = A_L + A_H$ ($Z = Z_L + Z_H$) is the mass (charge) number of fissioning nucleus. By taking into consideration the volume conservation, the shape of the system is defined by the mass and charge numbers of the fragments, the deformation parameters β_i ($i = L, H$), and interfragment distance R. The index $i = L$ or H. The potential energy [4,5]

$$\begin{aligned} U(A_i,Z_i,\beta_i,R) &= U_L^{LD}(A_L,Z_L,\beta_L) + \delta U_L^{\rm shell}(A_L,Z_L,\beta_L,E_H^*) \\ &\quad + U_H^{LD}(A_H,Z_H,\beta_H) + \delta U_H^{\rm shell}(A_H,Z_H,\beta_H,E_H^*) \\ &\quad + V^C(A_i,Z_i,\beta_i,R) + V^N(A_i,Z_i,\beta_i,R) \end{aligned} \quad (1)$$

of the DNS consists of the energies of the fragments (the liquid-drop energy U_i^{LD} plus deformation dependent shell-correction term $\delta U_i^{\rm shell}$) and energy $V = V^C + V^N$ of the fragment-fragment interaction. The interaction potential consists of the Coulomb interaction potential V^C of two uniformly charged ellipsoids and nuclear interaction potential in the double-folding form [4–6,29]. In the region of fission fragments considered, the interaction potential has a potential pocket and external barrier located at the distances of about (0.7–1.1) fm and (1.5–2) fm, respectively, between the tips of the fragments depending on deformations of the fragments. The internuclear distance R in Eq. (1) corresponds to the position $R = R_m(A_i,Z_i,\beta_i)$ of

 ©2018 American Physical Society

the minimum of this pocket. The decay barrier, $B_{qf}(A_i, Z_i, \beta_i)$, calculated as the difference of the potential energies at the bottom of the potential pocket $[R = R_m(A_i, Z_i, \beta_i)]$ and the top of the external barrier $[R = R_b(A_i, Z_i, \beta_i)]$, prevents the decay of the DNS in R. Note that the height of the barrier B_{qf} decreases with the charge asymmetry.

Because the thermal equilibrium is assumed at scission point, the excitation energy $E^*(A_i, Z_i, \beta_i, R_m) = E^*_{CN} + [U_{CN}(A, Z, \beta) - U(A_i, Z_i, \beta_i, R_m)]$ at scission is calculated as the initial excitation energy of the fissioning nucleus E^*_{CN} plus the difference between the potential energy $U_{CN}(A, Z, \beta)$ of the fissioning nucleus and one $U(A_i, Z_i, \beta_i, R_m)$ of the system at the scission point [4,5]. The excitation energies E^*_i in the DNS nuclei are assumed to be shared between the fragments proportionally to their masses.

The shell correction terms are calculated with the Strutinsky method and the two-center shell model [30]. The damping of these terms with excitation energy E^*_i is introduced as $\delta U^{\rm shell}_i(A_i, Z_i, \beta_i, E^*_i) = \delta U^{\rm shell}_i(A_i, Z_i, \beta_i, E^*_i = 0) \exp[-E^*_i/E_D]$, where $E_D = 18.5$ MeV is the damping constant. The relative formation-decay probability of the DNS with particular masses, charges, and deformations of the fragments is statistically calculated as follows [4,5]:

$$w(A_i, Z_i, \beta_i, E^*) = N_0 \exp\left[-\frac{U(A_i, Z_i, \beta_i, R_m) + B_{qf}(A_i, Z_i, \beta_i)}{T}\right], \quad (2)$$

where N_0 is the normalization factor. In Eq. (2), the temperature is calculated as $T = \sqrt{E^*/a}$, where $a = A/12$ MeV^{-1} is the level density parameter in the Fermi-gas model. In our calculations, a single value is used for the temperature at the global potential minimum of U before the shell damping. The term $\exp[-B_{qf}/T]$ describes the decay probability of the system. With increasing elongation and decreasing charge (mass) asymmetry the value of B_{qf} decreases, the system becomes more unstable and decays.

In order to obtain the mass-charge distribution of fission fragments, one should integrate Eq. (2) over β_L and β_H:

$$Y(A_i, Z_i, E^*) = N_0 \int d\beta_L d\beta_H w(A_i, Z_i, \beta_i, E^*). \quad (3)$$

The ratio of the yields of fragments with different charge/mass numbers is governed by the difference in energy and in width between the corresponding potential minima in the plane (β_L, β_H), as seen in Eq. (2). For two potential energy surfaces with the minima close in energy, a higher yield stems from the DNS with a wider and more shallow minimum, and a lower yield emerges from an abrupt and narrow minimum. This is a direct result of Eq. (3) [4,5]. Note that in the case of fast (slow) growth of the liquid-drop surface energy with increasing deformations, the minimum in the (β_L, β_H) plane is positioned at smaller (larger) deformations and is deep and narrow (shallow and wide).

For the calculations of mass and charge distributions, one should sum $Y(A_i, Z_i, E^*)$ over Z_i and A_i, respectively. As follows, the yield with mass A_L (charge Z_L) depends on the number of fragmentations with the same A_L (Z_L) but different Z_L (A_L).

The calculations were restricted only to even-even fission fragments which mainly define the shapes of the charge and mass distributions. The inclusion of the odd-even and odd-odd fission fragments can elucidate even-odd effects but can not appreciably change the smooth part of charge (mass) distributions in which we are interested in. The even-odd effects would add some oscillations to this smooth part. In order to obtain a smoother curve for the mass distribution and to simulate the minimal experimental uncertainty in the measurement of the mass number of the fission fragment, each calculated yield is smeared by the Gaussian with the width 1.5 amu [4–6,15,16]. At energies considered, we assume that the neutron emission prior to fission will not cause major change in the fission yield of isotopes of Fm and No.

The explanation of the asymmetric fission mode at high excitations by the multichance fission or fission after consecutive neutron evaporations is strongly model dependent and under discussion. As known from the experimental data [31], the number of pre-scission neutrons does not exceed 1–2 at excitation energies 50–60 MeV of heavy actinides. In nuclei considered the estimated fission barrier is smaller than neutron separation energy. Thus, the role of multichance fission is expected to be suppressed in these nuclei.

III. CALCULATED RESULTS

In Figs. 1–8, the calculated charge and mass distributions resulting from the spontaneous and induced fission of ^{254,256,258,260,264}Fm, ^{258,260,262,264}No, and ^{262,264,266}Rf isotopes are presented. The measured mass distributions [32–37] are well reproduced for the spontaneous fission of ^{254,256}Fm, ^{262}No, ^{262}Rf, and for the thermal-neutron-induced fission of ^{255,257}Fm. In the cases of fission of ^{254,256}Fm, the measured mass distributions present two asymmetric peaks as in our theoretical results. The peak-to-valley ratio decreases with increasing neutron number of Fm. In the fission of ^{262}No and ^{262}Rf, the measured [36,37] and calculated mass distributions are symmetric with the large widths. In contrast to the experimental data [3], the calculated mass distribution for ^{258}Fm is rather wide and has asymmetric bumps, even though the symmetric yields are extremely enhanced, and is strikingly similar to the experimental one for ^{257}Fm (Fig. 1) [2]. For ^{258}No (Fig. 5), the symmetric mass yields are larger than the asymmetric mass-yields that is in a good agreement with the experimental data [3].

The calculated charge distributions of spontaneous fission of ^{254,256,258,260,264}Fm have the asymmetric shape (Fig. 2). The tendency to a more symmetric charge splitting of fermium isotopes with increasing neutron number is clearly seen. In the case of the spontaneous fission of ^{258}Fm (Fig. 2), the charge distribution presents two peaks, with a small minimum for the symmetric Sn + Sn charge split. This is explained by the fact that the high yield of Cd ($Z_L = 48$) or Te ($Z_H = 52$) mainly originates from three mass fragmentations ^{122}Cd + ^{136}Te, ^{124}Cd + ^{134}Te, and ^{126}Cd + ^{132}Te which have almost the same potential energies U. The yields of symmetric charge split mostly originate from the ^{126}Sn + ^{132}Sn configuration, for which the potential energy U is larger by about 2 MeV than those for the Cd + Te configurations. There are two more

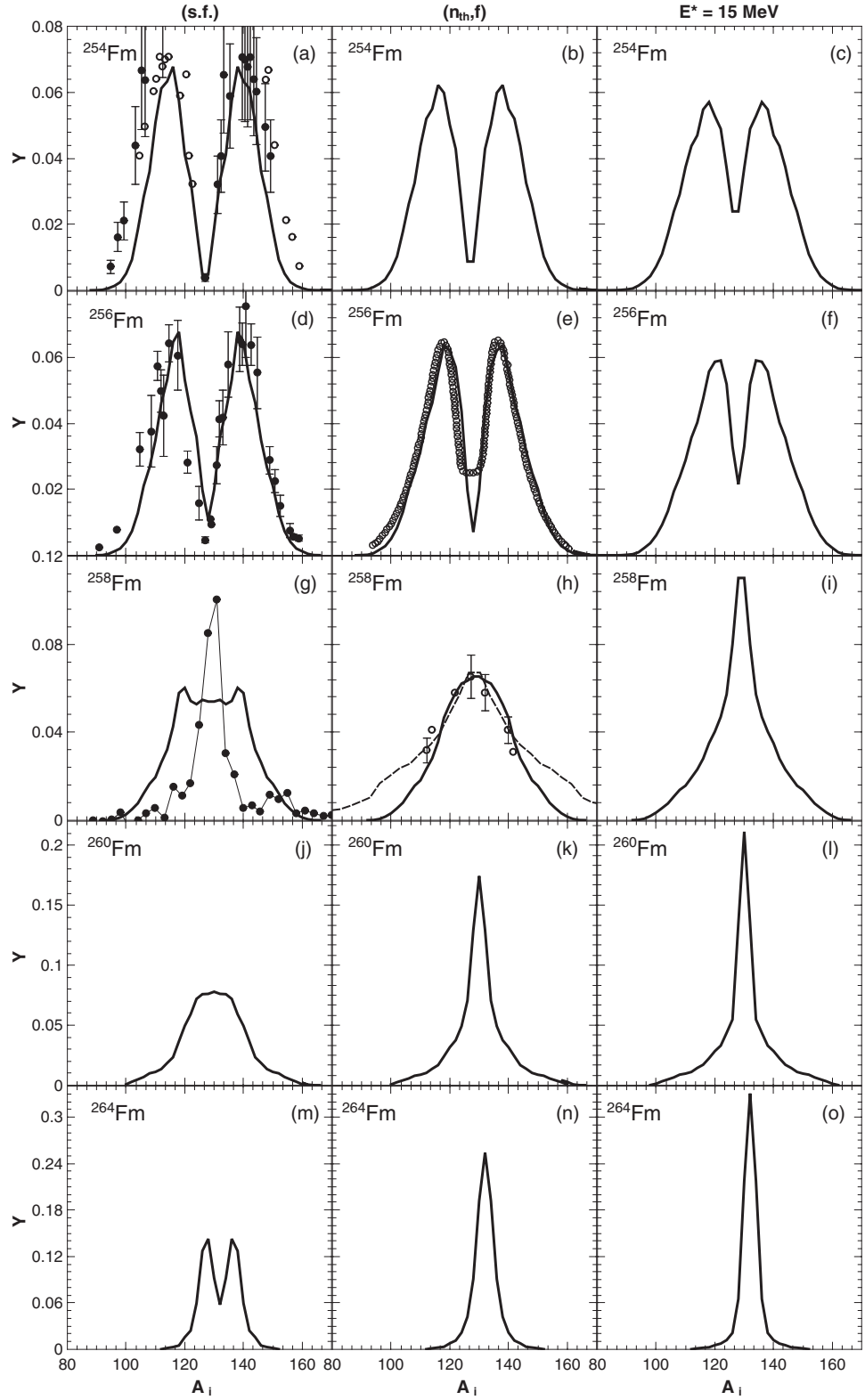

FIG. 1. The calculated mass distributions (solid lines) resulting from the spontaneous ($E^* = 0$ MeV, the first column) and induced ($E^* = 15$ MeV, the third column) fission of the indicated nuclei ^{254,256,258,260,264}Fm, and thermal-neutron-induced ($E^* \sim 6.3$ MeV, the second column) fission of nuclei ^{253,255,257,259,263}Fm. The calculations are performed for even-even mass and charge fragmentations. The distributions are normalized to unity. The open symbols represent experimental data of Refs. [3,32–35]. The spontaneous fission data for the ^{258}Fm were multiplied by the factor 0.8. In (h), the dashed line represents the provisional mass deduced in Ref. [35], and the open square represent radiochemically deduced secondary yield, while the open circles are the derived primary distributions [33].

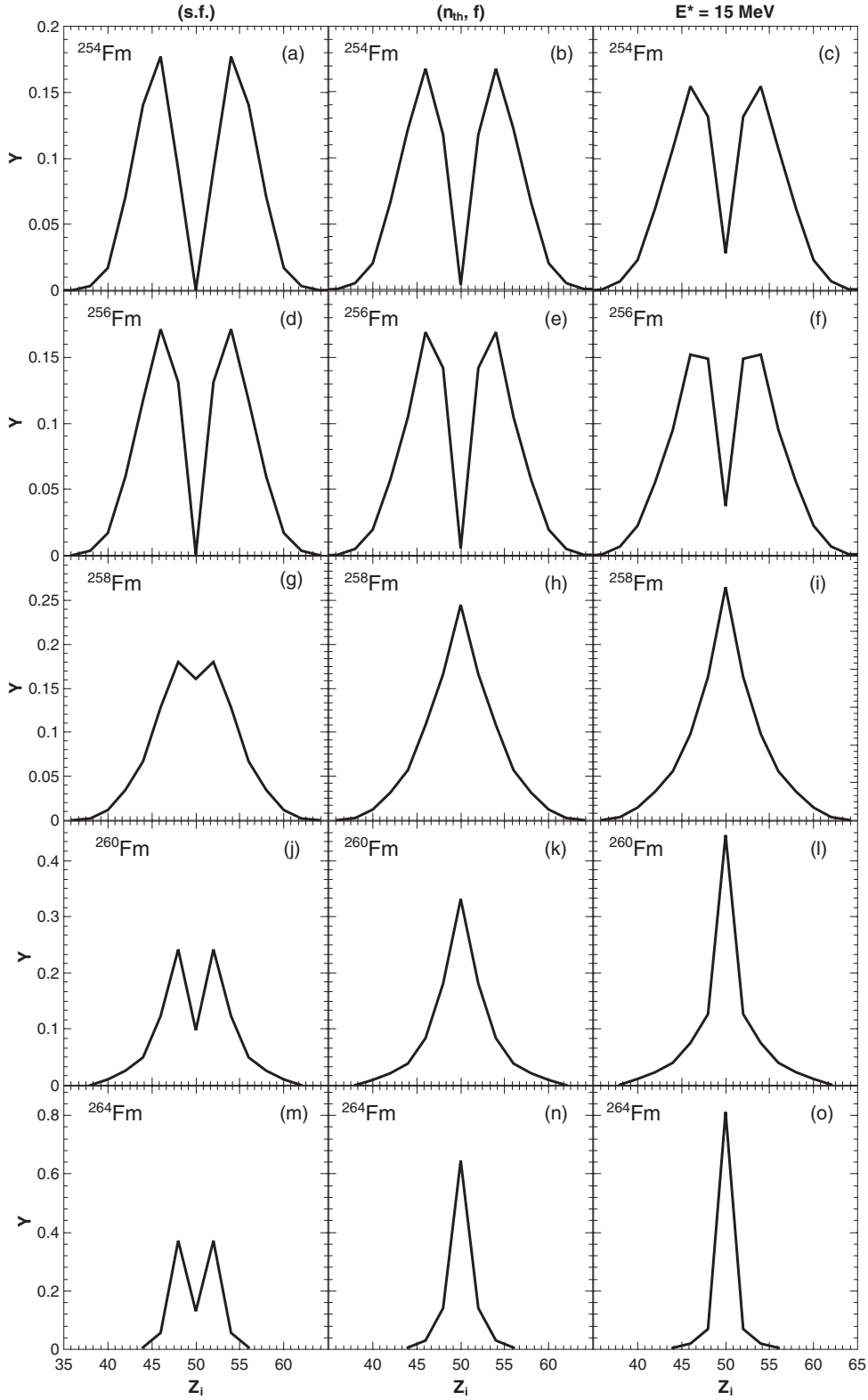

FIG. 2. The calculated charge distributions (solid lines) resulting from the spontaneous ($E^* = 0$ MeV, the first column) and induced ($E^* = 15$ MeV, the third column) fission of the indicated nuclei ^{254,256,258,260,264}Fm, and thermal-neutron-induced ($E^* \sim 6.3$ MeV, the second column) fission of nuclei ^{253,255,257,259,263}Fm. The calculations are performed for even-even mass and charge fragmentations. The distributions are normalized to unity.

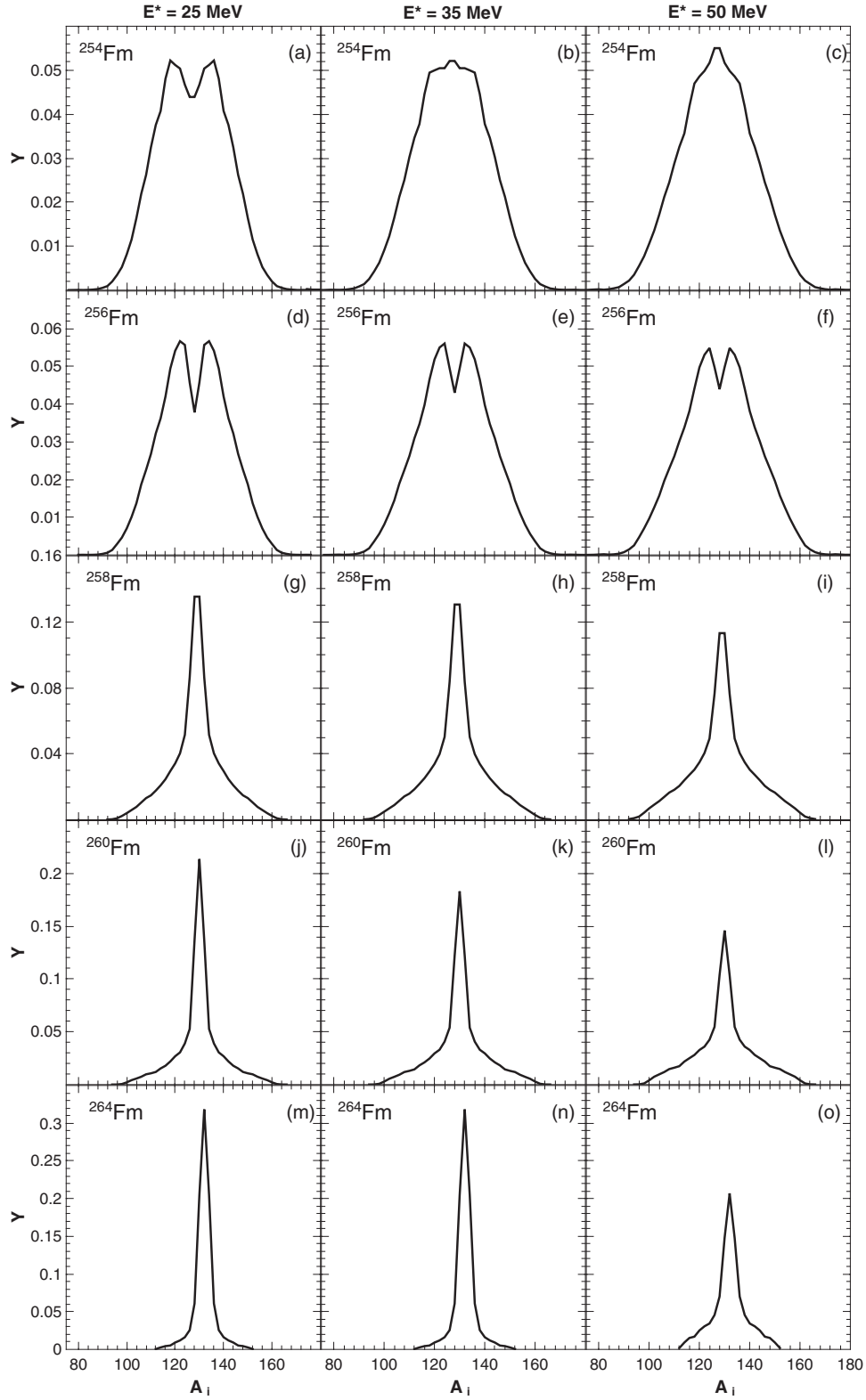

FIG. 3. The same as in Fig. 1, but for $E^* = 25$ MeV (the first column), $E^* = 35$ MeV (the second column), and $E^* = 50$ MeV (the third column) excitation energies.

mass fragmentations ^{124}Sn + ^{134}Sn and ^{128}Sn + ^{130}Sn which contribute to the symmetric yields. Because their potential energies are higher by 4 MeV and 3 MeV, respectively, than those for the Cd + Te configurations, their contributions to the symmetric yields are rather small. Note that our previously calculated charge distribution [6] of spontaneous fission of ^{258}Fm has to be corrected based on the present results.

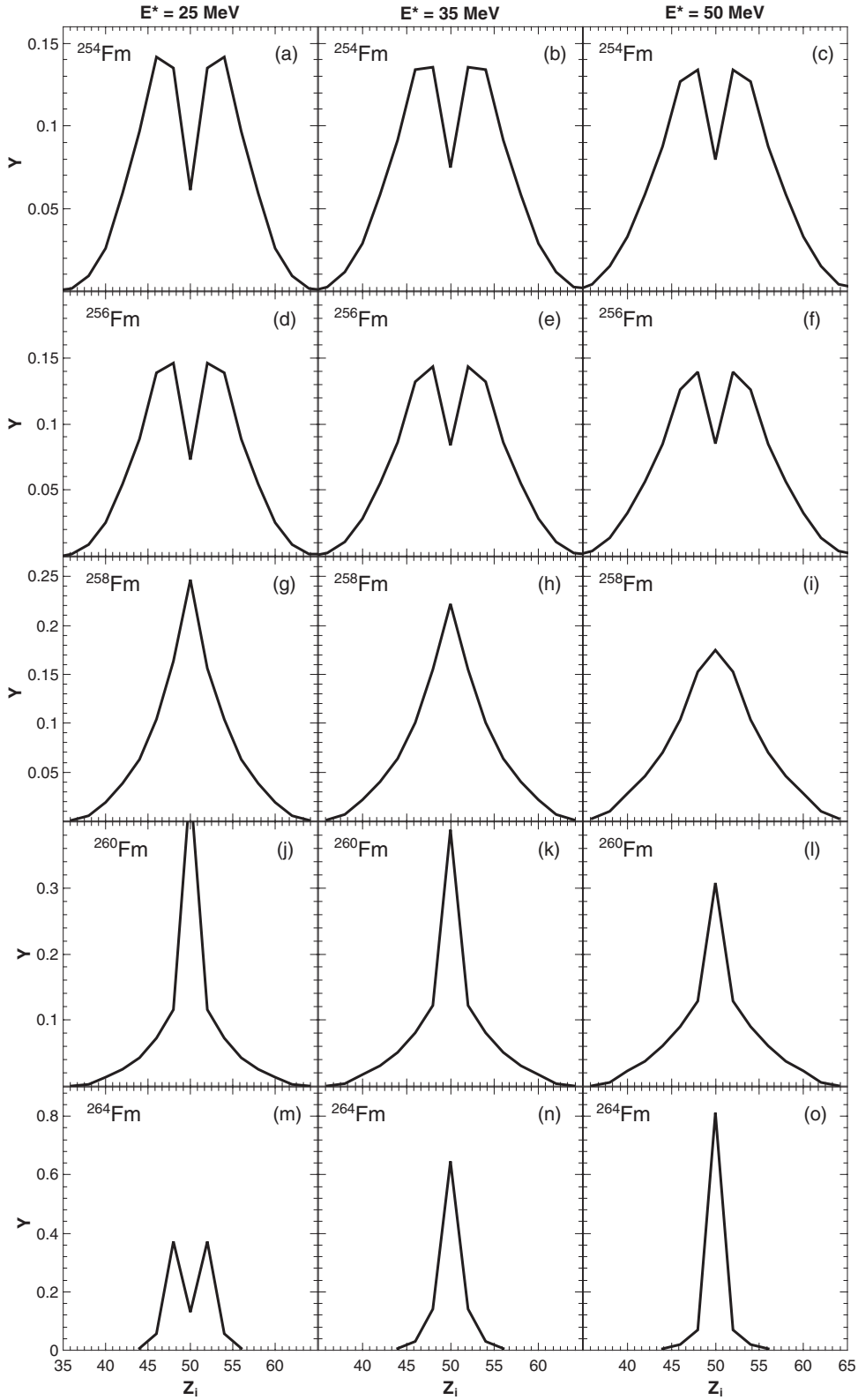

FIG. 4. The same as in Fig. 2, but for $E^* = 25$ MeV (the first column), $E^* = 35$ MeV (the second column), and $E^* = 50$ MeV (the third column) excitation energies.

As seen in Figs. 1 and 2, in the case of spontaneous fission of ^{260}Fm with the symmetric mass distribution, the charge distribution is asymmetric one with charge split Cd + Te. With increasing excitation energy the charge distribution becomes symmetric one (Figs. 2 and 4). For the thermal-neutron-induced fission of ^{257}Fm (Figs. 1 and 2), the experimental and calculated mass distributions are symmetric ones whereas the predicted charge distribution is asymmetric. However, at

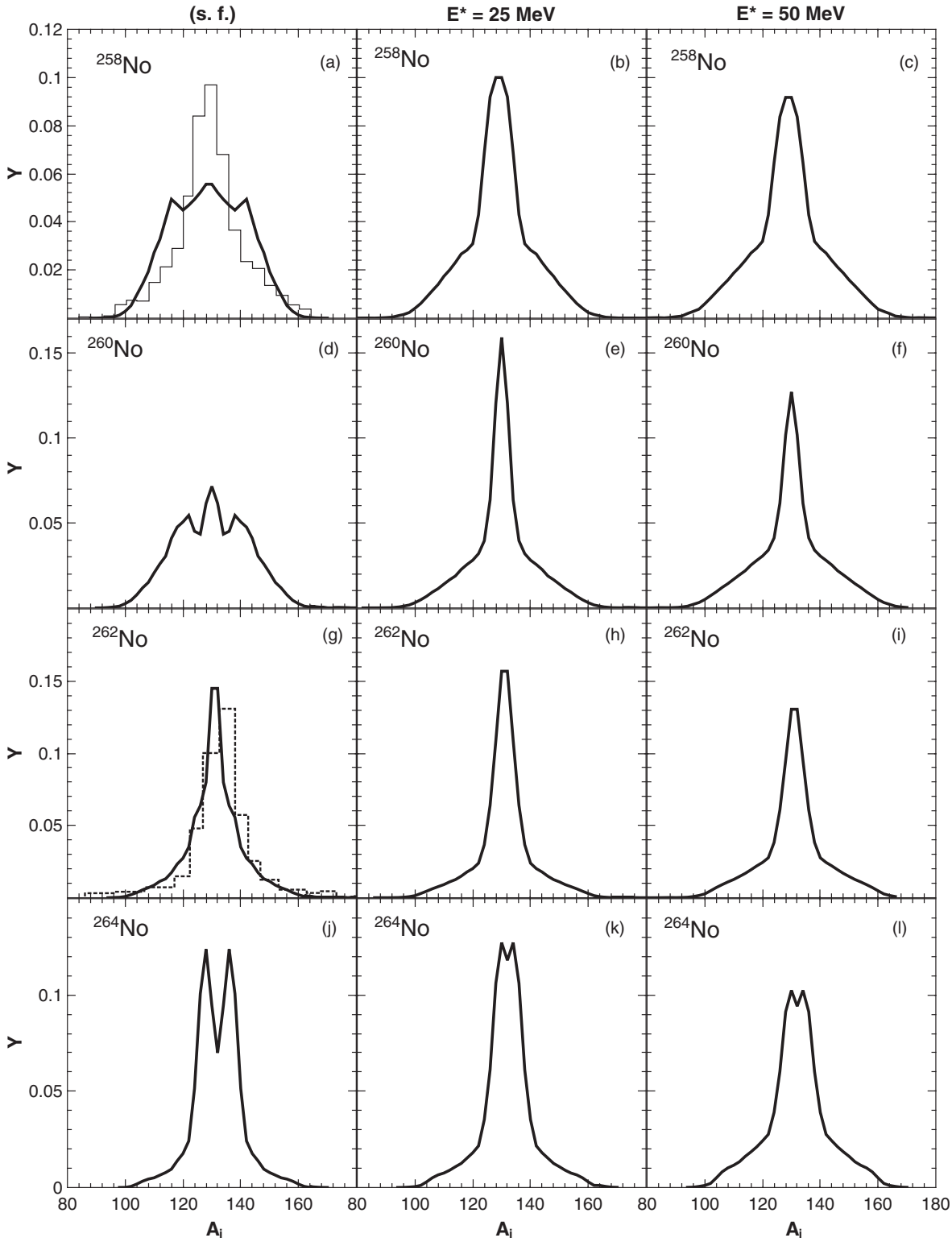

FIG. 5. The calculated mass distributions (solid lines) resulting from the fission of the indicated nuclei ^{260,262,264}No at excitation energies $E^* = 0$ MeV (the first column), $E^* = 25$ MeV (the second column), and $E^* = 50$ MeV (the third column). The calculations are performed for even-even mass and charge fragmentations. The distributions are normalized to unity. In (a) and (g), the histograms represent experimental data of Refs. [3] and [36], respectively.

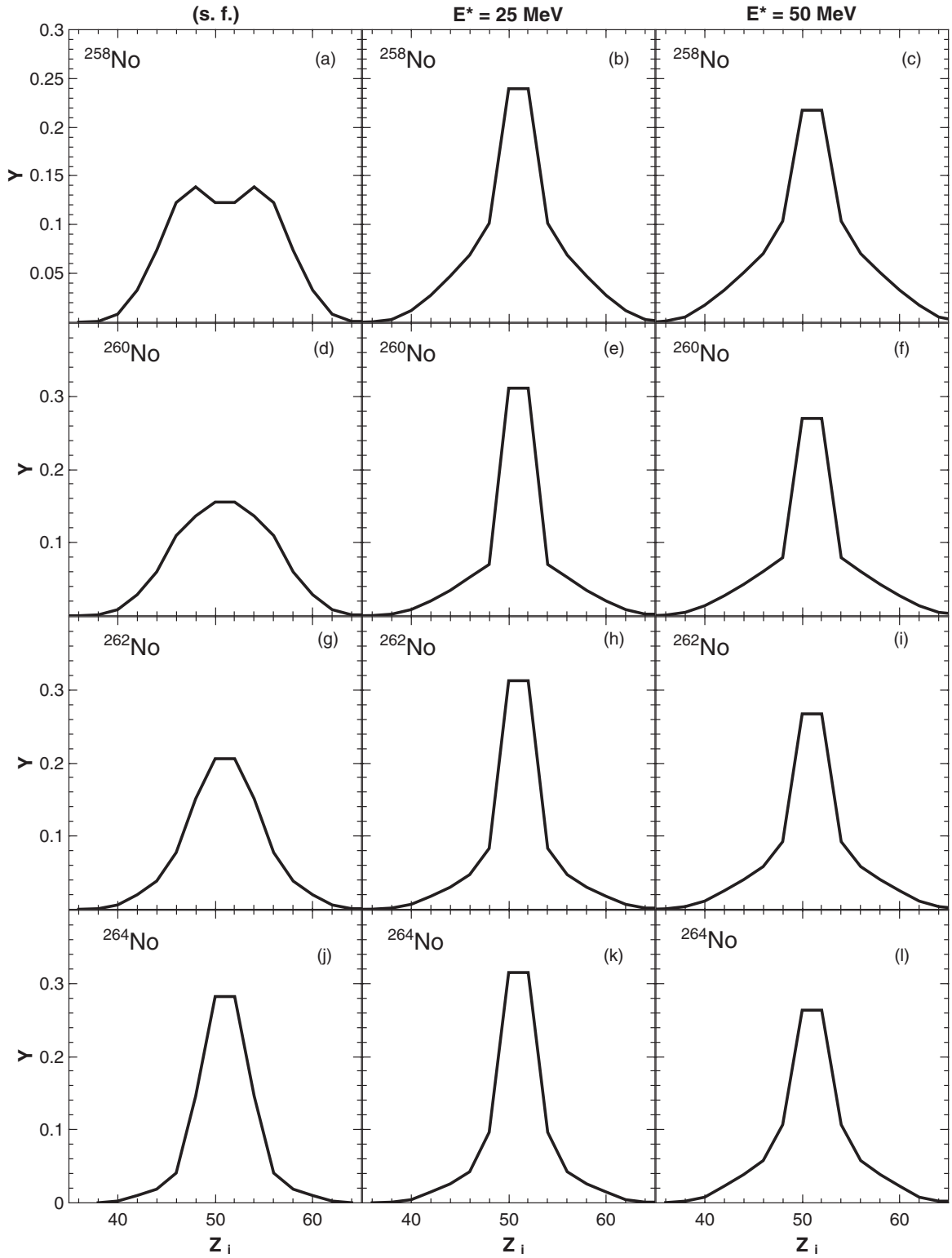

FIG. 6. The calculated charge distributions (solid lines) resulting from the fission of the indicated nuclei ^{260,262,264}No at excitation energies $E^* = 0$ MeV (the first column), $E^* = 25$ MeV (the second column), and $E^* = 50$ MeV (the third column). The calculations are performed for even-even mass and charge fragmentations. The distributions are normalized to unity.

$E^* \geqslant 15$ MeV the difference between these distributions vanish. For the induced fission of ^{254}Fm at $E^* = 35$ and 50 MeV (Figs. 3 and 4), the shape of mass yields becomes symmetric in contrast to one of the charge distribution. This unexpected difference between the shapes of mass and charge yields is worth to be studied experimentally. In the case of spontaneous fission of ^{260}No (Figs. 5 and 6), the mass distribution displays symmetric ($A_L = A_H = 130$) and asymmetric ($A_L = 122$, $A_H =$

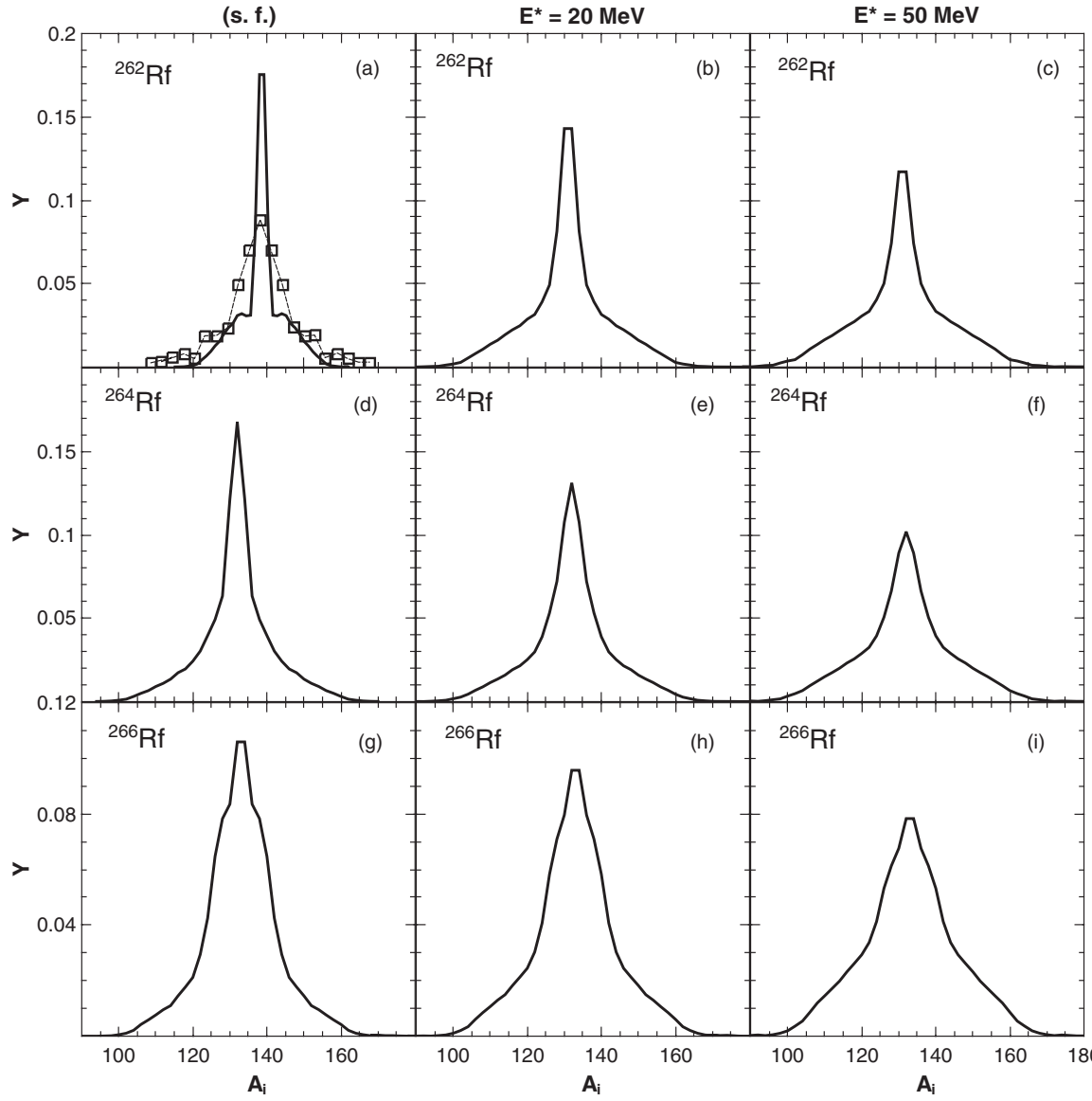

FIG. 7. The same as in Fig. 5, but for the indicated nuclei ^{262,264,266}Rf. In (a), the symbols connected by line represent the experimental data of Ref. [37].

138) peaks. For ^{260}No, the peaks of the charge distribution are at $Z_L = 50$ and $Z_H = 52$. The spontaneous fission of ^{264}No (Figs. 5 and 6) has the slightly asymmetric mass distribution with peaks at $A_L = 128$ and $A_H = 136$ and charge distribution with peaks at $Z_L = 50$ and $Z_H = 52$. For the spontaneous fission of ^{266}Rf (Figs. 7 and 8), the mass yield is symmetric and the charge-yield is asymmetric ($Z_L = 50$ and $Z_H = 54$). Note the in the case of spontaneous fission of ^{264}Fm (Figs. 1 and 2), the peaks of charge and mass distributions are at $Z_L = 48$, $Z_H = 52$ and $A_L = 128$, $A_H = 136$, respectively.

The interplay between the liquid-drop surface energy and the nucleus-nucleus interaction potential at scission is the main reason of the appearance or disappearance of the asymmetric fission mode. This interplay depends on the shell effects, excitation energy, and isospin of the fissioning nucleus. The shell effects affect directly and indirectly (through the deformations of nuclei) the appearance of the asymmetric minimum.

As a global trend for the isotopes of Fm and No, the symmetric components of the mass and charge yields are enhanced with increasing excitation energy (Figs. 1–6). The saturation of the symmetric components is reached at around 15–30 MeV. At larger E^* the distributions becomes wider. The fission of ^{260}No is a good example of that (Figs. 5 and 6). The shift to more symmetric mass and charge distributions and the saturation of the symmetric components with increasing excitation energy (Figs. 1–6) can be understood in the following way: for each mass and charge fragmentation the configurations with the highest yields correspond to local minima on the potential energy surfaces (β_L, β_H). These minima of the potential energy surface (PES) result from the tricky competition between the macroscopic interaction and liquid-drop (surface) energies, and the microscopic shell corrections at scission. The strong shells also affect the macroscopic parts of the potential energy by fixing the minimum energy at small deformations (β_L,

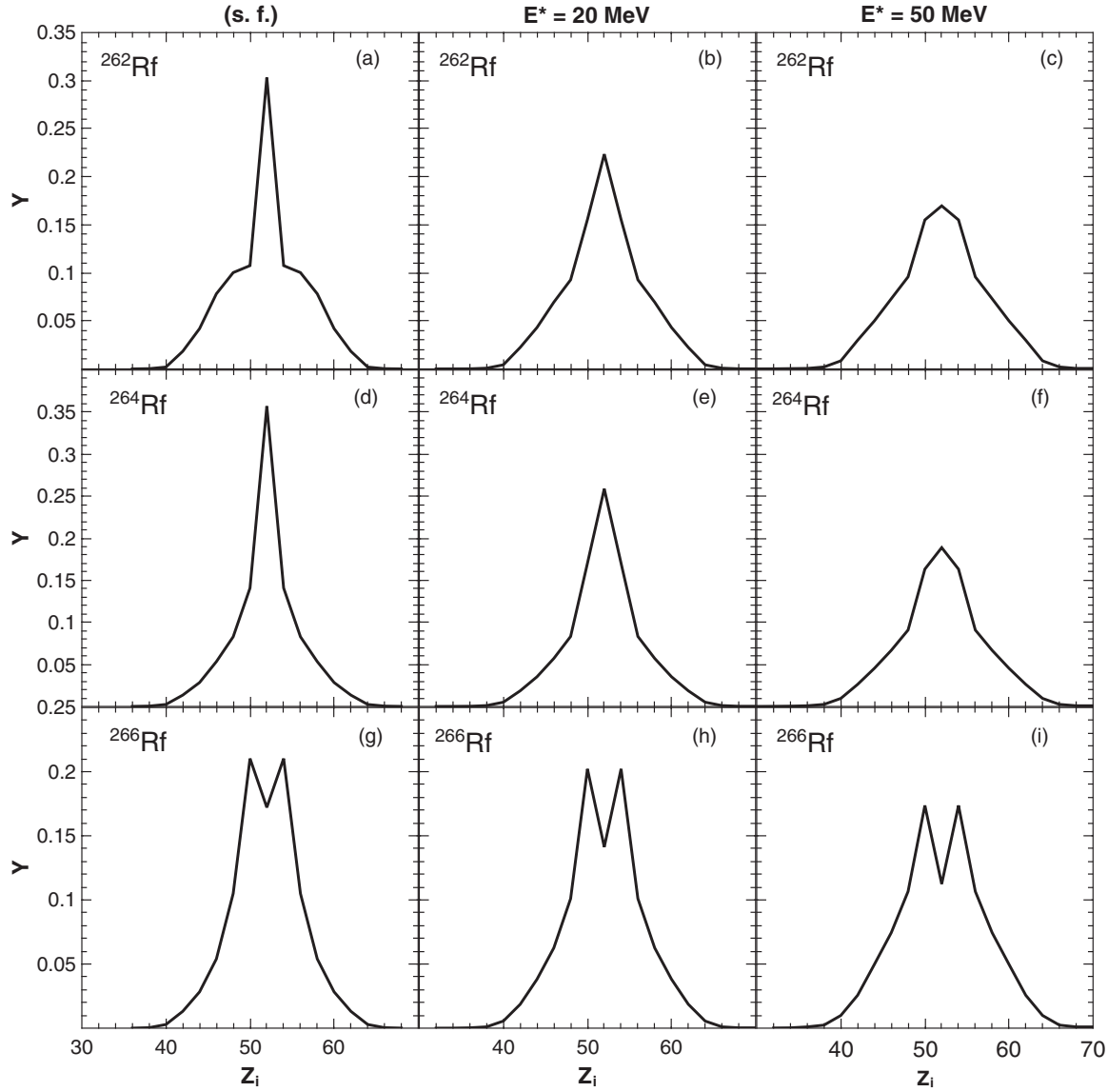

FIG. 8. The same as in Fig. 6, but for the indicated nuclei ^{262,264,266}Rf.

β_H). With increasing excitation energy, the shell effects are washed out, and the stiffness of the nuclear surface decreases. The combined effect is the enlargement of the minima on the PES and their shift towards much larger deformations. At large E^* the shell effects are completely damped, the surface stiffness becomes minimal, and the minima on the PES reach their maximum widths and final position. At this point the yields reach the maximal values, and further increase of excitation energy leads only to the population of more asymmetric accessible configurations.

In the case of fission of ^{262,264,266}Rf (Figs. 7 and 8), the increase of excitation energy leads to the access of previously inaccessible asymmetric configurations and to the decrease of the symmetric component.

IV. CONCLUSIONS

The mass and charge distributions resulting from the spontaneous and induced fission of even-even nuclei ^{254,256,258,260,264}Fm, ^{258,260,262,264}No, and ^{262,264,266}Rf were calculated within the statistical scission-point fission model. For these fissioning nuclei, the available experimental mass distributions in the spontaneous and thermal-neutron-induced fission were well described excepting ^{258}Fm(s.f.). In contrast to the experimental data, the calculated mass distribution for the spontaneous fission of ^{258}Fm is rather wide and has asymmetric bumps, even though the symmetric yields are extremely enhanced. However, the calculated spontaneous fission of ^{258}Fm shows slightly asymmetric charge distribution. In the case of spontaneous fission of ^{260}Fm, we found that the mass distribution is symmetric but the charge distribution are asymmetric ($Z_L = 48$, $Z_H = 52$). For ^{260}No(s.f.), the mass distribution has asymmetric and symmetric peaks and the charge distribution has peaks at $Z_L = 50$ and $Z_H = 52$. For ^{266}Rf(s.f.), the mass yield is symmetric and the charge yield is asymmetric ($Z_L = 50$ and $Z_H = 54$).

For the thermal-neutron-induced fission of ^{257}Fm, the asymmetric charge distribution ($Z_L = 48$, $Z_H = 52$) was predicted.

As well-known, the reaction ^{257}Fm(n_{th}, f) has the symmetric mass yield. For the fission of ^{254}Fm at $E^* = 35$ and 50 MeV, the symmetric shape of mass yields and the asymmetric shape of charge yields were obtained. For ^{260,262,264}No (^{266}Rf), the asymmetric peaks at $Z_L = 50$ and $Z_H = 52$ ($Z_L = 50$ and $Z_H = 54$) is conserved with increasing E^*. The experimental verifications of these theoretical predictions are desirable.

Our calculations for spontaneously fissioning nuclei Fm, No, and Rf suggest that an evolution of charge-yield shape occurs gradually with increasing isospin and excitation energy. For the isotopes of Fm and No, the symmetric components of mass and charge distributions are enhanced with increasing E^*. For the first time, we demonstrated that at some critical E^* the saturation of the symmetric yields occurs. The transformation of the shape of mass distribution occurs in a similar fashion like that of the charge distribution, but faster. For ^{254,256}Fm, the shape of charge yields evolves slower with increasing E^* than the shape of the mass yields and remains asymmetric even at high excitation energy ($E^* = 50$ MeV). In the fission of ^{258}Fm and ^{260}Fm, the symmetric component of the charge (mass) distribution is enhanced much faster with excitation energy due to the rapid transition from the strong shell-effect-governed to the macroscopic-governed symmetric fission behavior. Once the shell effects are damped at high excitation energy, the fission is strictly driven by the competition between the liquid-drop binding energy and the interaction energy of the two fragments. Any increase of excitation energy leads to the access of previously inaccessible asymmetric configurations. This, together with the smooth character of macroscopic energies, mainly leads to a saturation of the symmetric yields with increasing excitation energy and broadening of the mass and change distributions. Thus, the evolution of charge and mass distributions with the variation of excitation energy and isospin is related to the change of the PES at scission. The saturation effect is worth to be studied experimentally.

ACKNOWLEDGMENTS

This work was partially supported by the Romania-JINR(Dubna) Cooperation Programme, the Russian Foundation for Basic Research (Moscow), and DFG (Bonn). The work of N.V.A. was supported by Tomsk Polytechnic University Competitiveness Enhancement Program grant.

[1] D. C. Hoffman, D. M. Lee, K. E. Gregorich, M. J. Nurmia, R. B. Chadwick, K. B. Chen, K. R. Czerwinski, C. M. Gannett, H. L. Hall, R. A. Henderson, B. Kadkhodayan, S. A. Kreek, and J. D. Leyba, Phys. Rev. C **41**, 631 (1990); D. C. Hoffman, J. Alloys Compd. **213**, 67 (1994); S. Hofmann and G. Münzenberg, Rev. Mod. Phys. **72**, 733 (2000); A. N. Andreyev, M. Huyse, and P. Van Duppen, *ibid.* **85**, 1541 (2013).

[2] E. K. Hulet, R. W. Lougheed, J. H. Landrum, J. F. Wild, D. C. Hoffman, J. Weber, and J. B. Wilhelmy, Phys. Rev. C **21**, 966 (1980).

[3] E. K. Hulet, J. F. Wild, R. J. Dougan, R. W. Lougheed, J. H. Landrum, A. D. Dougan, P. A. Baisden, C. M. Henderson, R. J. Dupzyk, R. L. Hahn, M. Schadel, K. Sümmerer, and G. R. Bethune, Phys. Rev. C **40**, 770 (1989).

[4] H. Paşca, A. V. Andreev, G. G. Adamian, and N. V. Antonenko, Phys. Lett. B **760**, 800 (2016).

[5] H. Paşca, A. V. Andreev, G. G. Adamian, and N. V. Antonenko, Phys. Rev. C **94**, 064614 (2016).

[6] H. Paşca, A. V. Andreev, G. G. Adamian, and N. V. Antonenko, Nucl. Phys. A **969**, 226 (2018).

[7] B. D. Wilkins, E. P. Steinberg, and R. R. Chasman, Phys. Rev. C **14**, 1832 (1976).

[8] T. Matsuse, C. Beck, R. Nouicer, and D. Mahboub, Phys. Rev. C **55**, 1380 (1997).

[9] S. J. Sanders, A. Szanto de Toledo, and C. Beck, Phys. Rep. **311**, 487 (1999).

[10] S. Panebianco, J.-L. Sida, H. Goutte, J.-F. Lemaître, N. Dubray, and S. Hilaire, Phys. Rev. C **86**, 064601 (2012).

[11] M. Caamaño, F. Farget, O. Delaune, K. H. Schmidt, C. Schmitt, L. Audouin, C.-O. Bacri, J. Benlliure, E. Casarejos, X. Derkx, B. Fernández-Domínguez, L. Gaudefroy, C. Golabek, B. Jurado, A. Lemasson, D. Ramos, C. Rodríguez-Tajes, T. Roger, and A. Shrivastava, Phys. Rev. C **92**, 034606 (2015).

[12] A. V. Andreev, G. G. Adamian, N. V. Antonenko, S. P. Ivanova, and W. Scheid, Eur. Phys. J. A **22**, 51 (2004); **26**, 327 (2005).

[13] G. G. Adamian, N. V. Antonenko, and W. Scheid, in *Clusters in Nuclei*, Vol. 2, Lecture Notes in Physics 848, edited by Christian Beck (Springer-Verlag, Berlin, 2012), p. 165.

[14] A. V. Andreev, G. G. Adamian, and N. V. Antonenko, Phys. Rev. C **86**, 044315 (2012); A. V. Andreev, G. G. Adamian, N. V. Antonenko, and A. N. Andreyev, *ibid.* **88**, 047604 (2013).

[15] H. Paşca, A. V. Andreev, G. G. Adamian, N. V. Antonenko, and Y. Kim, Phys. Rev. C **93**, 054602 (2016); H. Paşca, EPJ Web of Conf. **107**, 07003 (2016).

[16] H. Paşca, A. V. Andreev, G. G. Adamian, and N. V. Antonenko, Eur. Phys. J. A **52**, 369 (2016).

[17] V. V. Volkov, Phys. Rep. **44**, 93 (1978); Izv. AN SSSR ser. fiz. **50**, 1879 (1986); *Nuclear Reactions of Deep Inelastic Transfers* (Energoizdat, Moscow, 1982); in *Treatise on Heavy-Ion Science*, edited by D. A. Bromley (Plenum Press, New York, 1989), Vol. 8, p. 255; Part. Nucl. **35**, 797 (2004).

[18] W. U. Schröder and J. R. Huizenga, in *Treatise on Heavy-Ion Science*, edited by D. A. Bromley (Plenum Press, New York, 1984), Vol. 2, p. 115.

[19] J. Randrup, Nucl. Phys. A **307**, 319 (1978); **327**, 490 (1979).

[20] G. G. Adamian, A. K. Nasirov, N. V. Antonenko, and R. V. Jolos, Phys. Part. Nucl. **25**, 583 (1994).

[21] S. Heinz *et al.*, Eur. Phys. J. A **38**, 227 (2008); **43**, 181 (2010); V. F. Comas *et al.*, *ibid.* **48**, 180 (2012); **49**, 112 (2013); S. Heinz *et al.*, *ibid.* **51**, 140 (2015).

[22] H. Q. Zhang, C. L. Zhang, C. J. Lin, Z. H. Liu, F. Yang, A. K. Nasirov, G. Mandaglio, M. Manganaro, and G. Giardina, Phys. Rev. C **81**, 034611 (2010).

[23] A. K. Nasirov, G. Mandaglio, G. G. Giardina, A. Sobiczewski, and A. I. Muminov, Phys. Rev. C **84**, 044612 (2011); K. Kim, Y. Kim, A. K. Nasirov, G. Mandaglio, and G. G. Giardina, *ibid.* **91**, 064608 (2015); G. Giardina, G. Mandaglio, A. K. Nasirov, A.

Anastasi, F. Curciarello, and G. Fazio, Nucl. Phys. A **970**, 168 (2018).

[24] N. Wang, E. G. Zhao, W. Scheid, and S. G. Zhou, Phys. Rev. C **85**, 041601(R) (2012); N. Wang, E. G. Zhao, and W. Scheid, *ibid.* **89**, 037601 (2014); L. Zhu, Z. Q. Feng, C. Li, and F. S. Zhang, *ibid.* **90**, 014612 (2014); X. J. Bao, Y. Gao, J. Q. Li, and H. F. Zhang, *ibid.* **91**, 064612 (2015); J. Q. Li, C. Li, G. Zhang, L. Zhu, Z. Liu, and F.-S. Zhang, *ibid.* **95**, 054612 (2017).

[25] Sh. A. Kalandarov, G. G. Adamian, N. V. Antonenko, and W. Scheid, Phys. Rev. C **82**, 044603 (2010); **83**, 054611 (2011); Sh. A. Kalandarov, G. G. Adamian, N. V. Antonenko, W. Scheid, and J. P. Wieleczko, *ibid.* **84**, 064601 (2011); Sh. A. Kalandarov, G. G. Adamian, and N. V. Antonenko, Phys. Part. Nucl. **43**, 825 (2012); Sh. A. Kalandarov, G. G. Adamian, N. V. Antonenko, and J. P. Wieleczko, Phys. Rev. C **90**, 024609 (2014); Sh. A. Kalandarov, D. Lacroix, G. G. Adamian, N. V. Antonenko, J. P. Wieleczko, S. Pirrone, and G. Politi, *ibid.* **93**, 024613 (2016).

[26] A. Shamlath, E. Prasad, N. Madhavan, P. V. Laveen, J. Gehlot, A. K. Nasirov, G. Giardina, G. Mandaglio, S. Nath, T. Banerjee, A. M. Vinodkumar, M. Shareef, A. Jhingan, T. Varughese, D. Kumar, P. S. Devi, Khushboo P. Jisha, N. Kumar, M. M. Hosamani, and S. Kailas, Phys. Rev. C **95**, 034610 (2017).

[27] J. Hong, G. G. Adamian, and N. V. Antonenko, Phys. Rev. C **92**, 014617 (2015); **94**, 044606 (2016); Eur. Phys. J. A **52**, 305 (2016); Phys. Lett. B **764**, 42 (2017).

[28] H. Paşca, Sh. A. Kalandarov, G. G. Adamian, and N. V. Antonenko, Phys. Rev. C **96**, 044611 (2017).

[29] G. G. Adamian *et al.*, Int. J. Mod. Phys. E **5**, 191 (1996).

[30] J. Maruhn and W. Greiner, Z. Phys. **251**, 431 (1972).

[31] D. Hilscher and H. Rossner, Ann. Phys. (France) **17**, 471 (1992).

[32] K. F. Flynn *et al.*, Phys. Rev. C **5**, 1725 (1972).

[33] K. F. Flynn *et al.*, Phys. Rev. C **12**, 1478 (1975).

[34] R. M. Harbour *et al.*, Phys. Rev. C **8**, 1488 (1973).

[35] W. John *et al.*, Phys. Rev. Lett. **27**, 45 (1971); R. C. Ragaini *et al.*, Phys. Rev. C **9**, 399 (1974).

[36] R. W. Lougheed, E. K. Hulet, K. J. Moody, J. F. Wild, R. J. Dougan, D. C. Hoffman, C. M. Gannett, R. A. Henderson, and D. M. Lee, in *Proceedings of the 3rd Chemistry Congress of North America* (Toronto, Canada, 1988); Nuclear Chemistry Division FY-1988 Annual Report Lawrence Livermore National Laboratory, UCAR-10062-88, 1988, p. 135.

[37] M. R. Lane, K. E. Gregorich, D. M. Lee, M. F. Mohar, M. Hsu, C. D. Kacher, B. Kadkhodayan, M. P. Neu, N. J. Stoyer, E. R. Sylwester, J. C. Yang, and D. C. Hoffman, Phys. Rev. C **53**, 2893 (1996).